



UNIVERSIDADE ESTADUAL DE CAMPINAS SISTEMA DE BIBLIOTECAS DA UNICAMP REPOSITÓRIO DA PRODUÇÃO CIENTIFICA E INTELECTUAL DA UNICAMP

Versão do arquivo anexado / Version of attached file:

Versão do Editor / Published Version

Mais informações no site da editora / Further information on publisher's website:

https://www.sciencedirect.com/science/article/pii/S2238785423029824

DOI: https://doi.org/10.1016/j.jmrt.2023.11.208

Direitos autorais / Publisher's copyright statement:

©2023 by Elsevier. All rights reserved.

ELSEVIER

Contents lists available at ScienceDirect

Journal of Materials Research and Technology

journal homepage: www.elsevier.com/locate/jmrt





HYbrid Titanium Alloys produced by laser powder bed Fusion using Ti-5553 and Ti-42Nb powder recycling

Gilberto V. Prandi^{*}, João Felipe Q. Rodrigues, Matheus Valentim, Márcio Sangali, Leticia F. Starck, Juliano Soyama, Rubens Caram

University of Campinas, School of Mechanical Engineering, Campinas, SP, Brazil

ARTICLE INFO

Handling Editor: L Murr

Keywords: Hybrid titanium alloy (HYTA) Powder recycling Additive manufacturing Laser powder bed fusion

ABSTRACT

Over the years, persistent investigations have been conducted in search of unique properties in the field of materials. In titanium alloys, this relentless pursuit is no exception, especially when aiming to combine often antagonistic characteristics such as ductility and high mechanical strength. Intending to achieve properties rarely obtainable through other processing methods, a new class of titanium alloys called HYbrid Titanium Alloys (HYTA) emerges. The primary objective of this study is to create a HYTA that harmonizes the ductility observed in Ti–42Nb with the characteristic mechanical strength of Ti-5553. To achieve this feat, the technique of Additive Manufacturing by Laser Powder Bed Fusion (AM by LPBF) was chosen to produce an alloy with 20 in wt. of Ti-5553. Additionally, considering the costs associated with powders for LBPF, the effect of incorporating recycled powders in the process was investigated. In this context, the effects of processing these powders were evaluated, analyzing the influence of morphology and oxygen content on the resulting samples. In this way, in addition to contributing to an in-depth understanding of Hybrid Titanium Alloys, it was possible to seek the optimization of costs associated with the AM technique. As a result, an alloy with unique properties was obtained with an ultimate tensile strength of 725 MPa and 24 % elongation in the as-built condition.

1. Introduction

In recent years, manufacturing processes have undergone significant transformation due to the emergence of novel approaches for producing three-dimensional parts and components. These innovative procedures rely on the deposition of materials layer by layer, a process known as Additive Manufacturing (AM). This technique involves several different processes, each one tailored to specific materials and requirements. The Laser Powder Bed Fusion (LPBF) method is the most used for metallic production, with excellent geometry accuracy for complex parts and improved surface finishing [1].

The LBPF technique is based on the sequential deposition of metallic powder layers, followed by selective laser melting following a two-dimensional pattern. The raw materials (pure metals or pre-alloyed) are supplied in hoppers, which control the deposition time. After material insertion into the chamber, a powder-laying device is applied to spread the powder on the bed, which is followed by laser scanning. As a result, a final unified solid material is obtained [4].

Besides its wide range of applications, the LPBF process still incurs high costs in terms of time, energy, and especially feedstock materials production price. Considering the growing demand for sustainable manufacturing, an alternative to mitigate the cost of this method could involve reusing previously processed powder. This is because during the LPBF process, as mentioned before, only a part of the spread material is melted. So, recycling and reusing the unmelted powder can be a viable solution to reduce material waste and overall production expenses, thus enhancing the sustainability of the method [5].

There are issues related to powder reutilization that should be considered, such as the degradation of powder circularity and the long-term pick up of atmospheric gases as interstitial elements, especially oxygen that severely affects the mechanical behavior of Ti-based materials [6]. Another concern regarding recycled powder is its flowability during the process, as it depends on powder circularity and moisture content. To deal with those difficulties, powder reused is employed, to some extent, mixed with virgin powder [17].

Recently, the LPBF has been intensively applied to process Ti alloys,

^{*} Corresponding author. Rua Mendeleiev, 200, Campinas, SP, 13083-860, Brazil. *E-mail address:* prandigv@gmail.com (G.V. Prandi).

 Table 1

 Nominal composition of individual powders according to the manufacturers.

Alloy	Nb [%]	Al [%]	V [%]	Mo [%]	Cr [%]	Fe [%]
Ti-42Nb	41.7	0.0	0.0	0.0	0.0	0.0
Ti-5553	0.0	4.4-5.7	4.0-5.5	4.0-5.5	2.5 - 3.5	0.3 - 0.5

including the Ti-5553 and Ti-42Nb alloys. While Ti-5553 alloy is a strong load-bearing material applied primarily in the aerospace industry [10], Ti-42Nb alloy is a biomedical Ti-based material that presents a low young modulus and high ductility [8].

Similar to composites, a combination of two different materials can result in a third material with enhanced properties. The combination of materials from two commercial Ti products is referred to as a Hybrid Titanium Alloy (HYTA) [25]. The Hybrid Titanium Alloys studied by Zafari et al. [23] allow the creation of a new class of titanium alloys. The heterogeneity of these alloys enables the formation of alloys whose properties differ from those of cp Ti and conventional Ti alloys. It's worth noting that these alloys can be produced from two or more titanium alloys and titanium classes (α , α - β and β) [24].

Based on the unique characteristics of these hybrid alloys, the objective of the present study was to combine the ductility of Ti–42Nb with the high mechanical strength of Ti-5553. Moreover, this was accomplished by powder reuse, a well-known challenge in Additive Manufacturing. Given the novelty of this new generation of Ti alloys, contributions to the understanding of microstructural formation mechanisms in LPBF were proposed.

2. Experimental procedure

The Ti-5553 and Ti–42Nb powders were recovered individually from the residue chamber after a previous additive manufacturing run and virgin powders of these materials were also prepared for comparison. These powders were produced by AP&C (Canada) and TaNiOBIS (Germany), respectively, through the gas atomization process. To remove particles larger than 63 μm , the powders were sieved for 2 h. The Ti-5553 and Ti–42Nb powder's nominal compositions are shown in Table 1.

A ratio of 80 % Ti–42Nb and 20 % Ti-5553 (in vol%) was used to achieve a ductile matrix of Ti–42Nb alloy with reinforcements of Ti-5553 alloy. The powders were mechanically mixed in an argon atmosphere at 140 RPM for 2 h, using a homemade designed eccentric mixer. The powders underwent five alternating purge cycles, consisting of

applying argon at a pressure of 1 bar for 10 min, increasing flowability through drying of possible atmospheric moisture added to the powder during handling, followed by a vacuum of 10^{-1} bar for the same duration.

To deepen the understanding of HYTAs, with a special focus on their formation mechanism, preliminary simulations were carried out. These simulations were conducted using the Thermo-Calc software in version 2023b, utilizing the specific TCTI4 database for titanium alloys.

The mixed powder was loaded into the feeding system of an OmniSint-160 LBPF machine, which is equipped with a Yb: YAG fiber laser system with a wavelength of 1070 nm, spot size of 80 μ m and maximum laser power of 400 W. Printing was performed in a highpurity argon flux atmosphere with an oxygen content below 200 ppm. The applied processing parameters were laser power (P) of 209 W, scan speed (V) of 700 mm/s, layer thickness (T) of 30 μ m and hatch distance (H) of 80 μ m, resulting in a volumetric energy density (Ev) of 124 J/mm³. This value of Ev was determined based on the preliminary analysis conducted by Sangali et al. [12]. The meandering technique with a 67° rotation of the laser scan direction after each deposited layer [9] was used for powder melting. All specimens were removed from the build platform and sliced with a Struers Accutom-10.

The metallic powder compositions were analyzed in a Shimadzu Xray fluorescence spectrometer (model EDX-7000). The interstitial oxygen and nitrogen contents were measured in Ti-5553 and Ti-42Nb virgin powders, as well as in the powder mixture obtained from the residues chamber, using a Leco TC400 analyzer. Furthermore, the same analyses were carried out on samples produced by manufacturing with virgin powders, tensile test specimens were also produced in Ti-5553 and Ti-42Nb for comparison. The microstructure was examined using a Zeiss EVO MA15 scanning electron microscope (SEM) equipped with an Energy-Dispersive X-ray spectroscopy (EDS) detector. The printed samples were ground, polished, and etched with Kroll solution (50 mL of HNO₃, 10 mL of HF, and 100 mL of H₂O). X-ray diffraction (XRD) analysis was performed on a PANalytical X'Pert diffractometer, utilizing $\text{CuK}\alpha$ radiation, 45 kV, and 35 mA, with 2θ ranging from 30° to 90° . This procedure was carried out both on the bulk as-built samples and the metallic powders. Bulk samples were analyzed under rotation to minimize texture effects.

Hardness tests were conducted using a Buehler 2100 equipment using a 500 gf load applied for 15 s. Nanoindentation tests were performed with a CSM Instruments Nanoindentation Tester (20 mN load applied for 5 s) equipped with a Berkovich diamond indenter. Tensile tests were carried out on an EMIC DL2000 universal testing machine

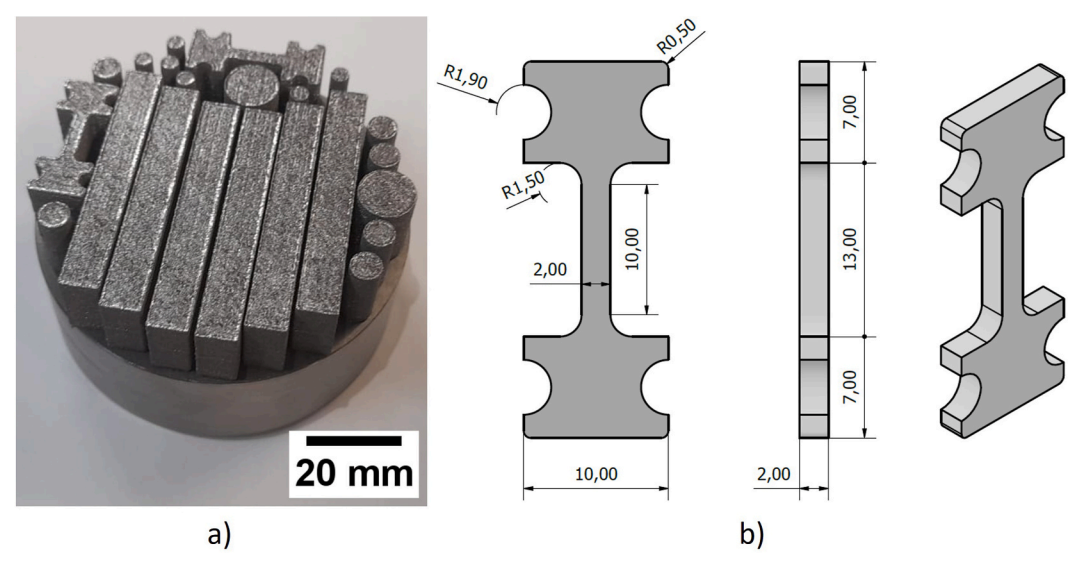


Fig. 1. a) Build produced by L-PBF, and b) drawing of the tensile test specimen.

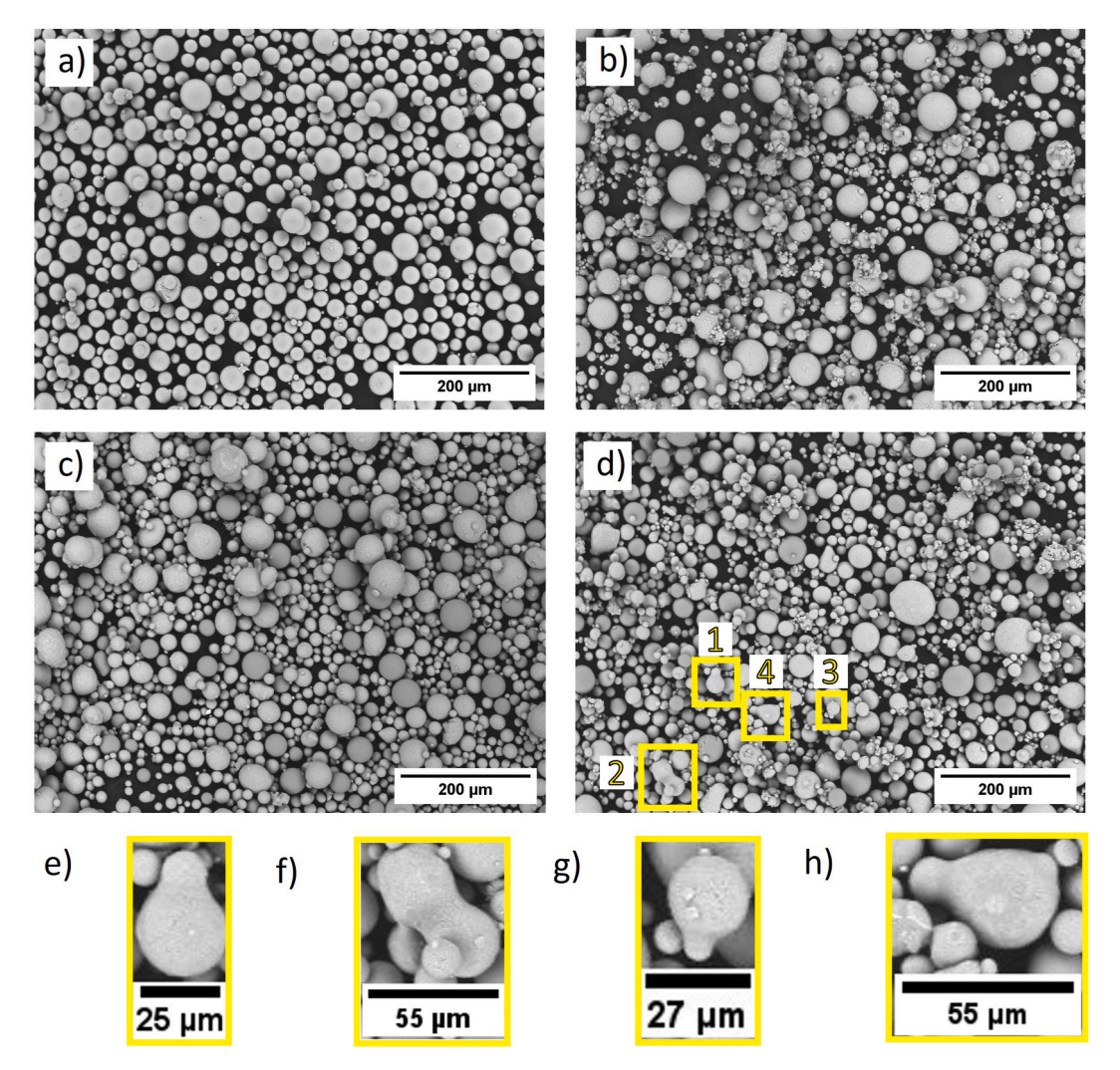


Fig. 2. SEM-BSE micrographs: (a) Virgin Ti-42Nb powder, (b) Virgin Ti-5553 powder, and (c) Recycled powder mixture. Images (d) to (g) show details of the sintered particles numbered in the image (c) from 1 to 4, respectively.

with a maximum capacity of 20 kN with a deformation rate of 1 mm/min, and deformation measurements were carried out using (DIC) Digital Image Correlation software and were obtained by testing the specimens illustrated in Fig. 1, which were designed following the standard's models the ISO/ASTM 52909:2022 standard. Tensile tests were carried out for both virgin and recycled materials. The measurements of the Young modulus were obtained through the pulse-echo ultrasound technique, utilizing the combination of longitudinal and transverse waves. Analyses were performed on samples with a thickness of 2 mm.

3. Results and discussion

3.1. Analysis of the raw materials

The powder morphological features were analyzed in the asreceived, virgin, and recycled mixture conditions. Fig. 2 shows the SEM images of the virgin and recycled powders. Fig. 2 a displays the Ti-5553 powders with a spherical form. Fig. 2 b indicates that the Ti-42Nb powders predominantly exhibited a spherical morphology, with some elongated particles and several satellites. Fig. 2 c and Fig. 2 d present a virgin and recycled mixture of the morphologies of the Ti-42Nb and Ti-5553 powders respectively. Additionally, the presence of previously spherical particles fused in the mixture is depicted in Fig. 2e-g, showing the sintering neck effect. This effect in powder recycling has already been reported by Araújo et al. [2], which occurs due to the heat transfer

in the powder originated by the consecutive laser application, reaching a temperature that is not sufficient to completely melt the materials but can promote points of metallurgical connection. This phenomenon has been observed and linked to powder reuse, as suggested, and observed by Gorgji et al. [5]. However, the sintering neck formation and its dynamics were discussed and simulated by several researchers, as described in Refs. [20,21]. It is important to understand that a high volume of powder with sintering necks can be detrimental to the additive manufacturing process, as it may lead to the formation of porosity during processing, as pointed out by Wang et al. [18].

Quantitative analyses were conducted to assess the size distribution of the as-received, virgin, and recycled powders. This evaluation was based on SEM images that were further subjected to image processing using the open-source ImageJ software. The results related to particle size distribution are presented in Fig. 3 a. The Ti-5553 particles show a slightly larger size compared to Ti–42Nb, with an average diameter of $19~\mu m$, and the majority fell within the range of $10{-}32~\mu m$. For Ti–42Nb, the average particle size was found to be $10~\mu m$, with most particles ranging from 2 to $29~\mu m$, and the largest particle reaching $45~\mu m$.

In the virgin and recycling powder mixture, an intermediate scenario was observed. The most particles ranged from 2 to 30 μm and from 3 to 30 μm for virgin and recycled powder, respectively. In the same way, the average diameter was 16 μm for the virgin powder and 12 μm for the recycled powder. Comparing the distribution of the powder sizes of the virgin and recycled powders, a reduction of D_{50} in the recycled powder

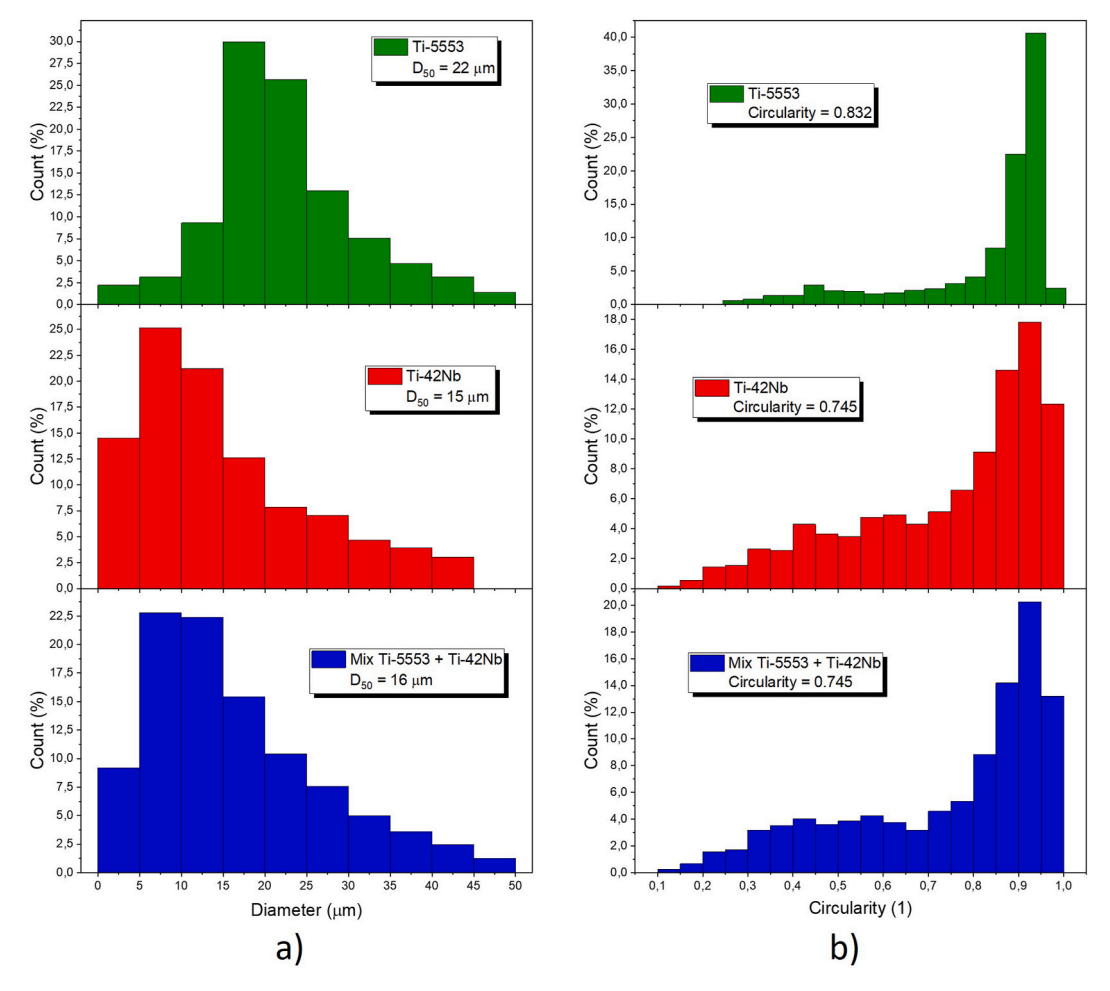


Fig. 3. Quantitative analysis of Ti-42Nb and Ti-5553 powders performed from SEM-BSE micrographs magnified 200x, showing in the left column (a) the distribution of average particle size and in the right column (b) the circularity of the powder particles.

Table 2
Analysis of oxygen and nitrogen contents in Ti–42Nb and Ti-5553 powders, both in materials acquired directly from the manufacturer, as well as in mixtures resulting from powder recycling and as-built samples.

Virgin materials					
Ti-42Nb powder		Ti-5553 powder		As built specimen	
O [%]	N [%]	O [%]	N [%]	O [%]	N [%]
0.239 ± 0.009 Recycled materials	0.0142 ± 0.0007	0.156 ± 0.009	0.0127 ± 0.0005	0.260 ± 0.010	0.0033 ± 0.0004
Recycled powder mix			As built specimen		
O [%] 0.286 ± 0.002	$\begin{array}{c} N \text{ [\%]} \\ 0.0160 \pm 0.0003 \end{array}$	-	O [%] 0.289 ± 0.004		N [%] 0.0221 ± 0.0003

is observed. It's suggested that this occurred due to the sieving process performed on the recycled powder to eliminate larger sintered particles, which consequently removed larger particles that were present in the virgin powder. In Fig. 3b, a particle circularity analysis was performed, confirming the findings of the qualitative analysis presented in Fig. 3. The Ti-5553 particles exhibited remarkable circularity, reaching a significant value of 0.880. Ti–42Nb, in turn, demonstrated considerable circularity, recording an index of 0.797. In the case of both virgin and recycled mixtures, there is proximity in circularity values, marking 0.827 and 0.811, respectively. It is noteworthy that in recycled powders a slight decrease in circularity was observed, an effect attributed to sintered powders.

A significant increase in the oxygen content of reused powders has been reported in the literature, which limits the maximum amount of possible recycling runs [17]. Additionally, titanium has a strong chemical affinity with oxygen, which can lead to an oxide layer at certain temperatures, leading to undesired effects in mechanical behavior. Therefore, the powders were quantitatively analyzed in the as-received and recycled conditions, as well as after the additive manufacturing process. Table 2 reveals that the oxygen and nitrogen content in the recycled powder was slightly higher than the levels found in the virgin Ti-5553 powder while being slightly lower than the content present in the Ti-42Nb powder. This discrepancy arises due to the concentrations of each element. However, the balance is not precise, partly due to an

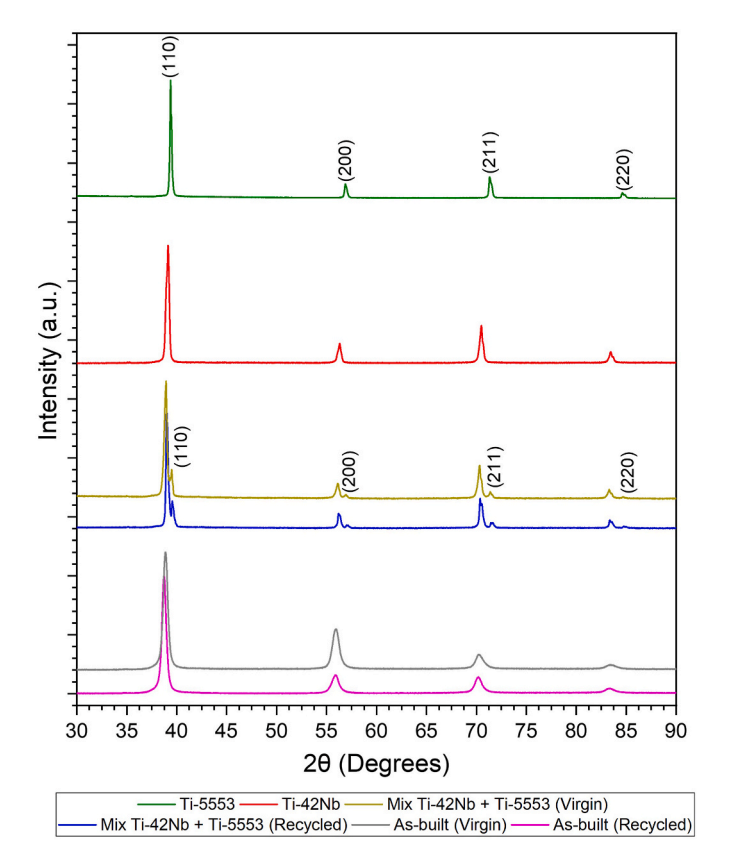


Fig. 4. XRD analyses performed on virgin metallic powders of Ti–42Nb, Ti-5553, recycled powder mixture, and as-built specimens from virgin and recycled powders.

increase caused by the absorption of oxygen during sintering. As for the material in its as-built form, a significant increase in oxygen content is observed, resulting from the entrapment of gases occurring during the sintering process, the increase was smaller for virgin powders, as reused powders retain a fraction of the oxygen from the additive manufacturing process.

The analysis of metallic powders using X-ray diffraction (XRD) indicated a shift in the diffraction peaks of Ti-42Nb and Ti-5553 alloys, according to Fig. 4. This was due to the differences in their lattice parameters. Measurements yielded values of 3.24 Å for Ti-5553 and 3.29 Å for Ti-42Nb, resulting in a rightward shift of the Ti-5553 peak in the XRD pattern. Furthermore, both powders exhibited only β -phase. The peaks in the mixture obtained from virgin powders are slightly broader compared to those in the recycled counterpart. This observation suggests that the broader distribution of diameters in the virgin powders is responsible for this outcome. It is crucial to highlight that there were no additional peaks identified in the recycled powders that were not originally present in the virgin samples. In both as-built samples produced by virgin and recycled powders, the presence of the β -phase was exclusively observed due to the high cooling rates during the AM process. Additionally, compared to the precursor powders, there was an observable peak broadening, due to the solid solution effect in the β-phases of Ti-5553 and Ti-42Nb.

The previous analyses conducted by X-ray Fluorescence Spectrometry indicated that the samples produced through additive manufacturing contained 24.1 $\%\pm0.1$ in the weight of Ti-5553 in virgin mixture powder and 22.1 $\%\pm0.1$ in the weight of Ti-5553 in recycling mixture powder. However, due to the technique's difficulty in measuring light elements such as aluminum and the discrepancies found in the quantification by X-ray diffraction (DRX), area-based EDS analyses were performed to obtain a more accurate quantification of the proportion of Ti–42Nb and Ti-5553 in the produced samples.

3.2. Analysis of the as-built specimens

The metallographic preparation of the samples was conducted both longitudinally, within the sample construction orientation, and transversely, in the direction of powder deposition during production, as illustrated in Fig. 5. It is worth noting that the magnification difference in the images was applied to obtain a representative area, as the formation of Ti-5553-rich regions varies in each building direction.

Examining the sample area through EDS analysis, the average contents of the investigated alloy were determined. For the mixture containing virgin powders, a composition of 78.0 $\%\pm0.1$ for Ti–42Nb and 22.0 $\%\pm0.3$ for Ti-5553 was observed. In the case of the mixture with recycled powders, the values were 78.8 $\%\pm0.1$ for Ti–42Nb and 21.2 $\%\pm0.7$ for Ti-5553 in the alloy. These results indicate equivalence within the associated uncertainties.

The variation between the techniques was expected given the intrinsic nature of uncertainty in each approach. Considering this variability, an average was calculated using the data from each technique, aiming for a more faithful representation of the actual composition present in the sample. Consequently, these findings revealed a content of 77.0 % \pm 0.4 for Ti–42Nb and 23.1 % \pm 0.4 for Ti-5553 in the alloy manufactured with virgin powders. For the alloy produced with recycled powders, the results indicated a content of 78.4 % \pm 0.4 for Ti–42Nb and 21.7 % \pm 0.8 for Ti-5553.

This disparity corresponds to a variation of 3.8 % for the alloy with the higher fraction and about 13.3 % for the alloy with the lower fraction in the material. In the sample manufactured with recycled powders, this disparity is slightly lower, below 2.1 % for Ti–42Nb and less than 7.7 % for Ti–5553, with this deviation related to the values of the initial powder mixture.

The formation of pure Ti–42Nb areas surrounded by Ti-5553-rich regions was frequently observed. To assess the compositional distribution in these islands, a point EDS analysis was carried out in different regions on an SEM-BSE micrograph, as shown in Fig. 6.

A mapping using EDS also allowed for better visualization of the formed islands, as shown in Fig. 7. The elemental map distribution and composition in Fig. 6 indicates that the bright regions were rich in Ti–42Nb, while the dark ones were rich in Ti-5553.

3.3. The microstructural formation of HYbrid titanium alloys (HYTA) by LPBF

When analyzing the EDS mapping in Fig. 7, it can be observed that Ti-5553 surrounded regions of pure Ti-42Nb. This was due to two main events. Firstly, there is a significant difference in the melting points of the two materials. Ti-42Nb has a higher melting point, being approximately 2469 $^{\circ}$ C [16]. On the other hand, Ti-5553 has a lower melting point, around 1630 $^{\circ}$ C [15], which causes it to melt more easily, forming a liquid matrix in which the Ti-42Nb particles were immersed.

The immersion of Ti–42Nb particles in the liquid matrix occurred due to the second event related to differences in the surface tension of the molten alloys. As illustrated in the curves in Fig. 8, also simulated using Thermo-Calc, there is a significant variation in the surface tensions of both alloys at the same temperature. This difference creates a convective regime due to the Marangoni effect, causing Ti–42Nb, which shows a higher surface tension, to descend while Ti-5553 remains on the surface of the molten pool, as mentioned in Ref. [24] and simulated for additive manufacturing by Rehman et al. [11]. This explains the metallographic difference between the longitudinal and transverse sections of the sample, as shown in Fig. 5. The simulation started at the onset of the first liquid phase formation.

Fig. 9 schematically describes the effects involved in microstructural formation in the Ti-5553 and Ti-42Nb hybrid alloy. It is proposed that the Marangoni force acting on the molten pool destabilizes it propelling spatter material towards the mushy zone. This region is located between the solidification front and the liquid under the laser's path and is caused

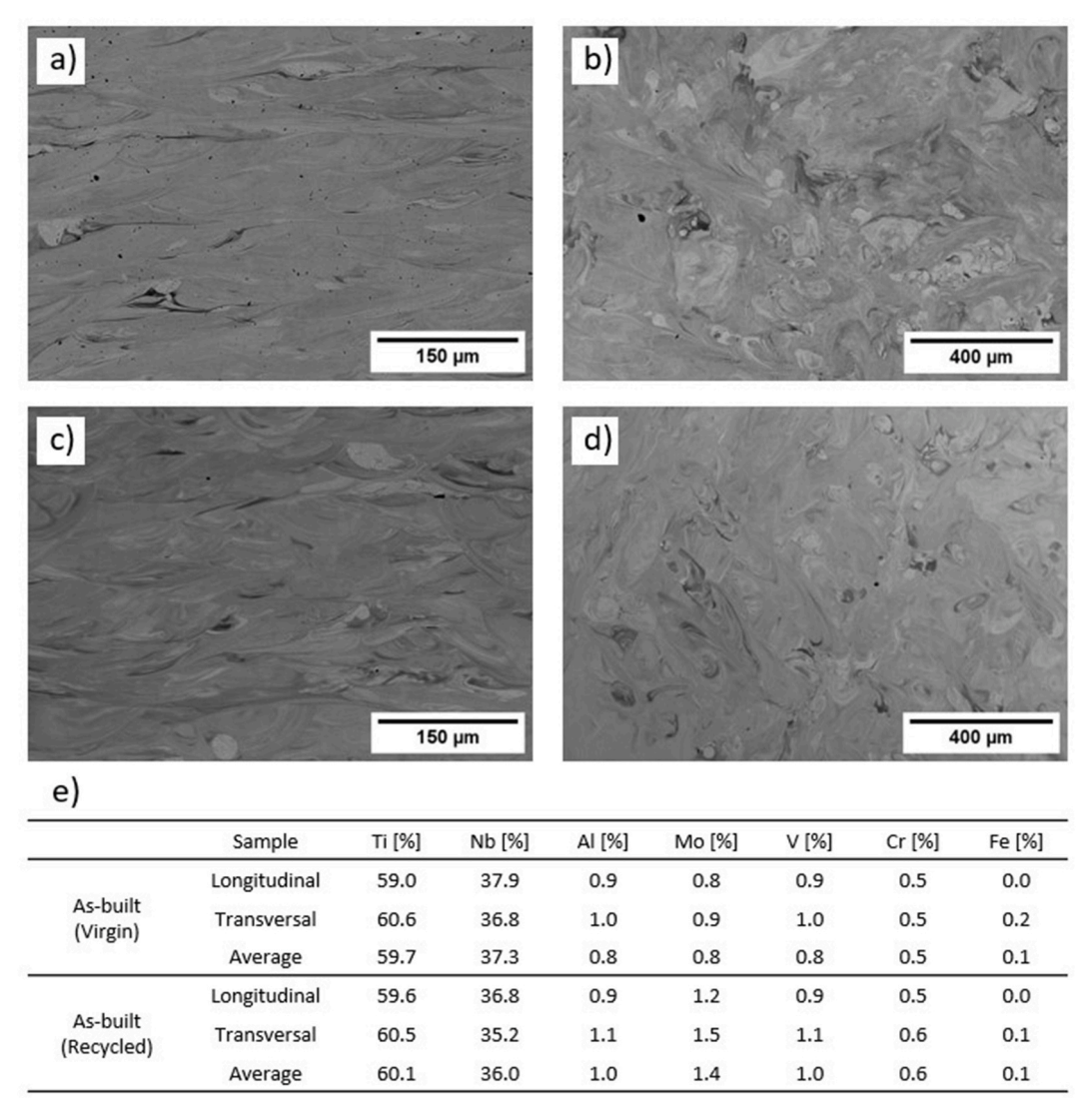


Fig. 5. SEM-BSE micrographs of L-PBF specimens: (a) and (b) depict the longitudinal and transverse sections, respectively, for as-built specimens manufactured with virgin powders. Similarly, (c) and (d) showcase the longitudinal and transverse sections for as-built specimens manufactured with recycled powders. The compositional values obtained by EDS are presented in (e).

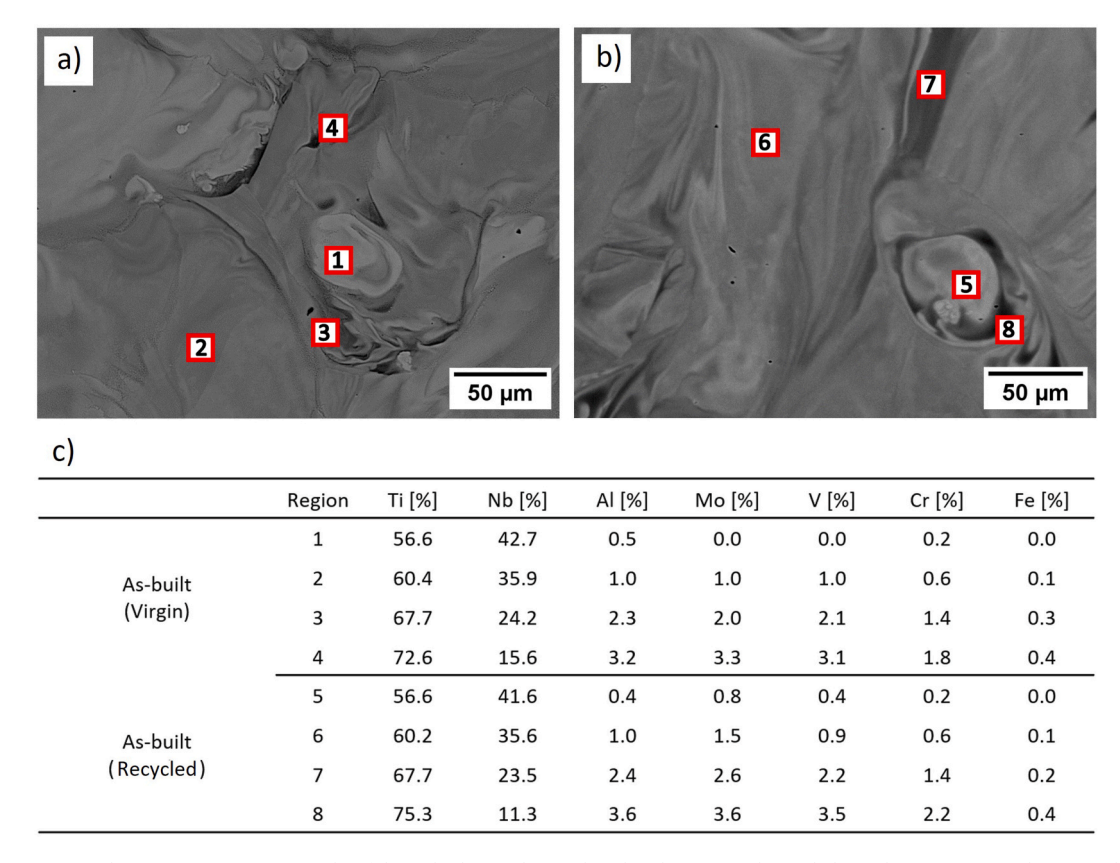


Fig. 6. SEM-BSE region analysis using EDS. Micrographs of the as-built samples produced with virgin and recycled powders are presented in (a) and (b) respectively, with numerically labeled regions indicating the points where EDS analyses were performed. In (c), a table showcases the compositions of each region marked in (a) and (b).

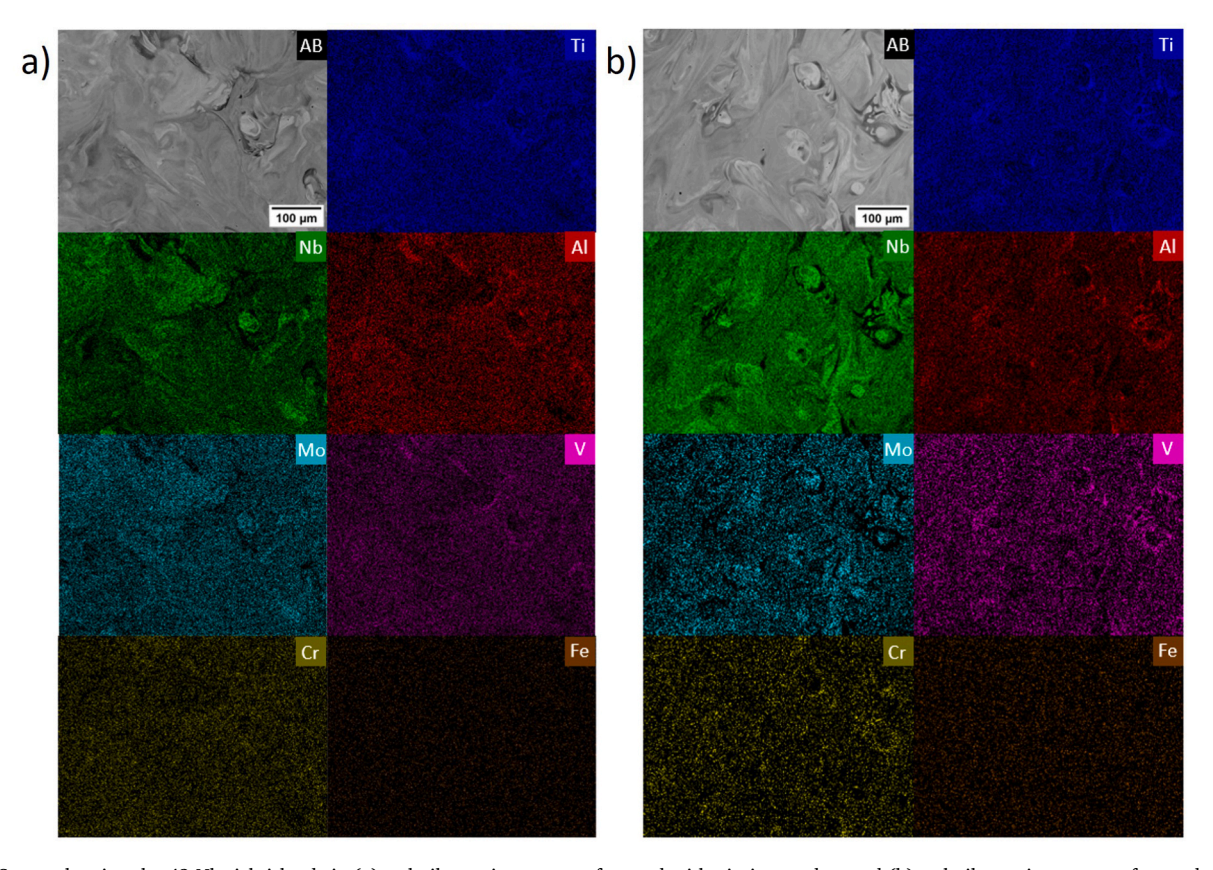
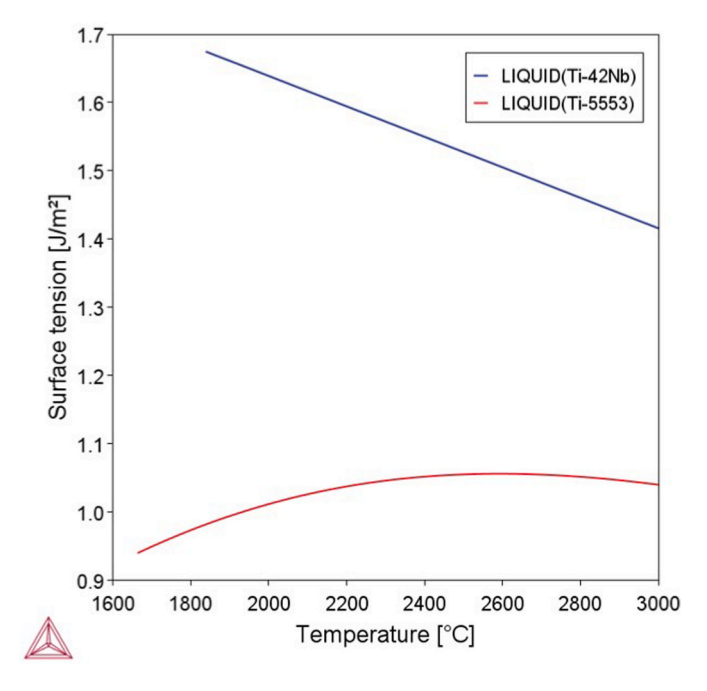


Fig. 7. EDS map showing the 42 Nb-rich islands in (a) as-built specimens manufactured with virgin powders and (b) as-built specimens manufactured with recycled powders.



 $\textbf{Fig. 8.} \ \, \textbf{Surface tension versus temperature of Ti-42Nb} \ \, \textbf{and Ti-5553 simulated using Thermo-Calc.}$

by the Plateau-Rayleigh effect as described and simulated in Refs. [19, 22], which results in a thermal loss. The surface tension and melting point difference lead to unmelted zones containing the higher melting point material and, consequently, the formation of regions that segregate as islands. This creates regions with partially sintered spatters and unmelted powder of this material, as shown in Fig. 12 c) and d).

3.4. Mechanical properties

The material density was determined following the ASTM B311:2022 standard, as image-based porosity analyses showed densification exceeding 98 % in as-built specimens manufactured with virgin and recycling powders. The density tests resulted in a value of $5.42\pm0.01~\text{g/cm}^3$ and $5.38\pm0.01~\text{g/cm}^3$ for as-built specimens manufactured with virgin and recycled powders respectively. Additionally, hardness with 500 gf (micro) and 20 mN (nano) analyses were performed, as illustrated in Fig. 10 b. Fig. 10 a. qualitatively illustrates the influence of each region on the performed indentation. The Berkovich indentations are larger in the Ti–42Nb region than in the Ti-5553, suggesting higher hardness in the Ti-5553 region. It is also noteworthy that no statistically significant differences between regions of the virgin and recycled samples related to micro and nano hardness were observed.

A higher hardness was measured in the Ti-5553 region compared to the Ti-42Nb region, which was expected due to their different mechanical behavior. The Ti-42 presents a high β stabilizing content that provides a high level of ductility when compared to the Ti-5553 alloy. Another factor contributing to this disparity arises from the lattice strain induced by the atomic size mismatch of the Ti-5553 alloy constituents as proposed by Zhang et al. [26].

Tensile curves of samples fabricated with virgin and recycled powders are depicted in Fig. 11. The variations in the curves were attributed to the material's heterogeneity resulting in regions with different levels of ductility. The heterogeneity evident in the curve's accounts for the distinct stiffness values found. As illustrated in Figs. 6 and 7, there was a significant compositional variation in the sample. Consequently, samples with a higher content of Ti-5553 exhibited higher stiffness.

Table 3 presents a comparative analysis between Ti-42Nb and Ti-5553 alloys, produced through additive manufacturing (AM) using both virgin and recycled powders, along with the average values obtained from the tensile curves of the hybrid alloy investigated in this study. Concerning the Ti-42Nb matrix, an increase in the elastic modulus was observed, as anticipated, attributed to the Ti-5553 alloy, which shows a higher stiffness [3]. This increase is also observed

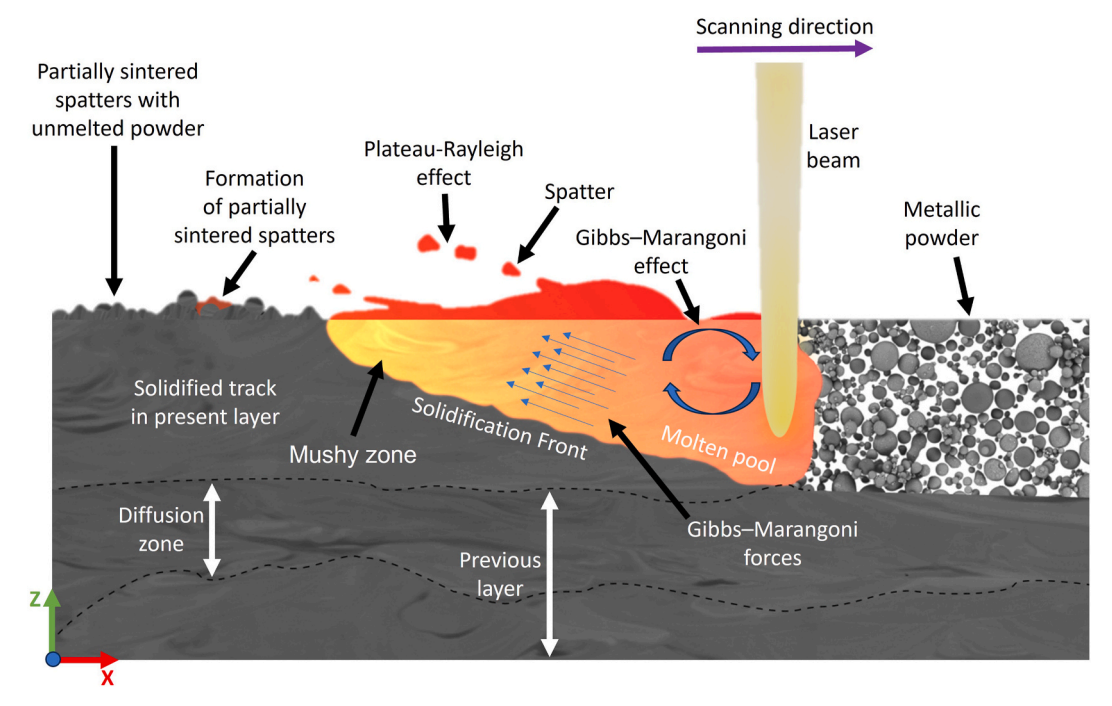


Fig. 9. Schematic overview of the effects involved in the formation of HYbrid Titanium Alloys in LPBF.

	Mix Ti-5553 + Ti-42Nb		b (Virgin)	Mix Ti-555	53 + Ti-42Nb (Recycled)	
100			Micro			Micro
and	Nano hardness		hardness	Nano hardness		hardness
Will the first the same of the	(Load: 20 mN)		(Load: 500	(Load: 20 mN)		(Load: 500
A SAN PLANTING AND THE TANK A SAN TH			gf)			gf)
	Regions	Regions		Regions	Regions	
STATE OF THE PROPERTY OF THE PARTY OF THE PA	rich in Ti-	rich in Ti-	Bulk	rich in Ti-	rich in Ti-	Bulk
	42Nb	5553		42Nb	5553	
The state of the s	$281.3 \pm$	330.2 ±	210.2 ±	$289.9 \pm$	343.6 ±	209.1 ±
10 μm	22.9	19.3	3.9	22.9	22.8	4.8
a)			b)		

Fig. 10. Microstructure image (a) showing the Berkovich indentations in both Ti-5553 (dark) and Ti-42Nb (light) rich regions. In (b), values of Vickers hardness in different regions of the build.

between virgin and recycled alloy blends, suggesting it is due to additional oxygen. There was also an increase in the yield strength and tensile strength, attributed to the incorporation of Ti-5553 as a reinforcing element in the hybrid alloy. It is worth noting that, due to uncertainties encountered, the yield strength in the recycled material is statistically equivalent to that of the virgin material, which is not the case for the maximum tensile strength, slightly higher for the recycled material. Moreover, there is a considerable increase in strength in the as-built condition of the hybrid alloy compared to Ti-42Nb. The high elongation capacity in both conditions is a result of the undersized sample geometry, as suggested by previous studies conducted by Moura et al. [7]. For the same reason, measurements of Young's modulus were conducted using the ultrasound technique.

Considering the similarity in the results obtained between the material produced from recycled and virgin powders, fractography analysis was performed exclusively on the recycled sample. The aim was to deepen the understanding of the morphology and the response to the test in this specific context.

Fracture analysis was conducted as illustrated in Fig. 12 a. This image was captured with a stereoscope and shows a characteristic fracture of ductile materials with a necking of the fracture region (also visible in the image), which is consistent with the Ti-42Nb matrix. The ductile nature of the fracture was confirmed in Fig. 12 b that shows an SEM-SE image of dimples at the fracture surface, as indicated by the yellow arrows. Furthermore, in Fig. 12c and d, the unmelted Ti-42Nb particles were analyzed using two different detectors, SEM-SE, and SEM-BSE. Both images were subjected to EDS analysis to confirm the presence of the unmelted powder. These particles might act as stress concentration points, potentially serving as crack nucleation sites, thus impairing their strength.

4. Conclusions

The potential of preparing hybrid Ti alloys with Ti-5553 and Ti-42Nb through Laser Powder Bed Fusion using recycled powders has been shown. However, precautions must be taken regarding the postrecycling oxygen content, as a single reprocessing cycle increases its levels. Additionally, morphological changes were observed. Moreover, an explanation for the microstructural formation involving the surface tension and Gibbs-Marangoni convection was proposed, which elucidated the formation of Nb-rich islands.

Mixing 20 wt% of Ti-5553 and 80 wt% of Ti-42Nb resulted in modifications of the mechanical properties, such as increased hardness in regions rich in Ti-5553 and overall improved strength in comparison

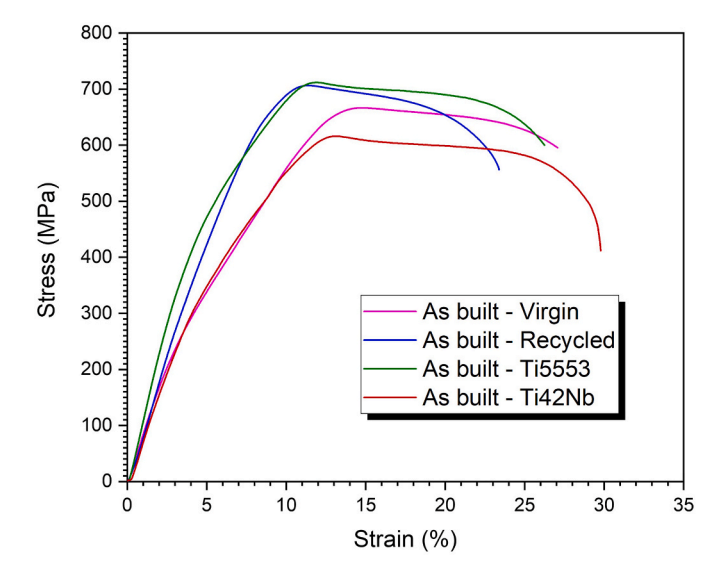


Fig. 11. Tensile curves of the as-built HYTA produced with recycled and virgin powders.

to Ti-42Nb. In the as-built condition, the hybrid alloy showed a tensile strength of 725 MPa with 24 % ductility. Considering that Ti-5553 alloy responds exceptionally well to aging heat treatment [14], future research will concentrate on subjecting this Ti-5553 and Ti-42Nb hybrid alloy to heat treatments, potentially leading to more substantial enhancements in mechanical strength.

When examining both virgin and recovered alloys, discrepancies in mechanical properties are evident, including an increase in hardness, elastic modulus, as well as maximum tensile and yield strengths. However, it is crucial to emphasize that, despite these variations, a substantial improvement is maintained compared to the Ti-42Nb alloy, which is predominantly present in the studied HYTA's. This phenomenon suggests that hybrid alloys derived from recovered materials hold significant potential for further in-depth studies and practical applications.

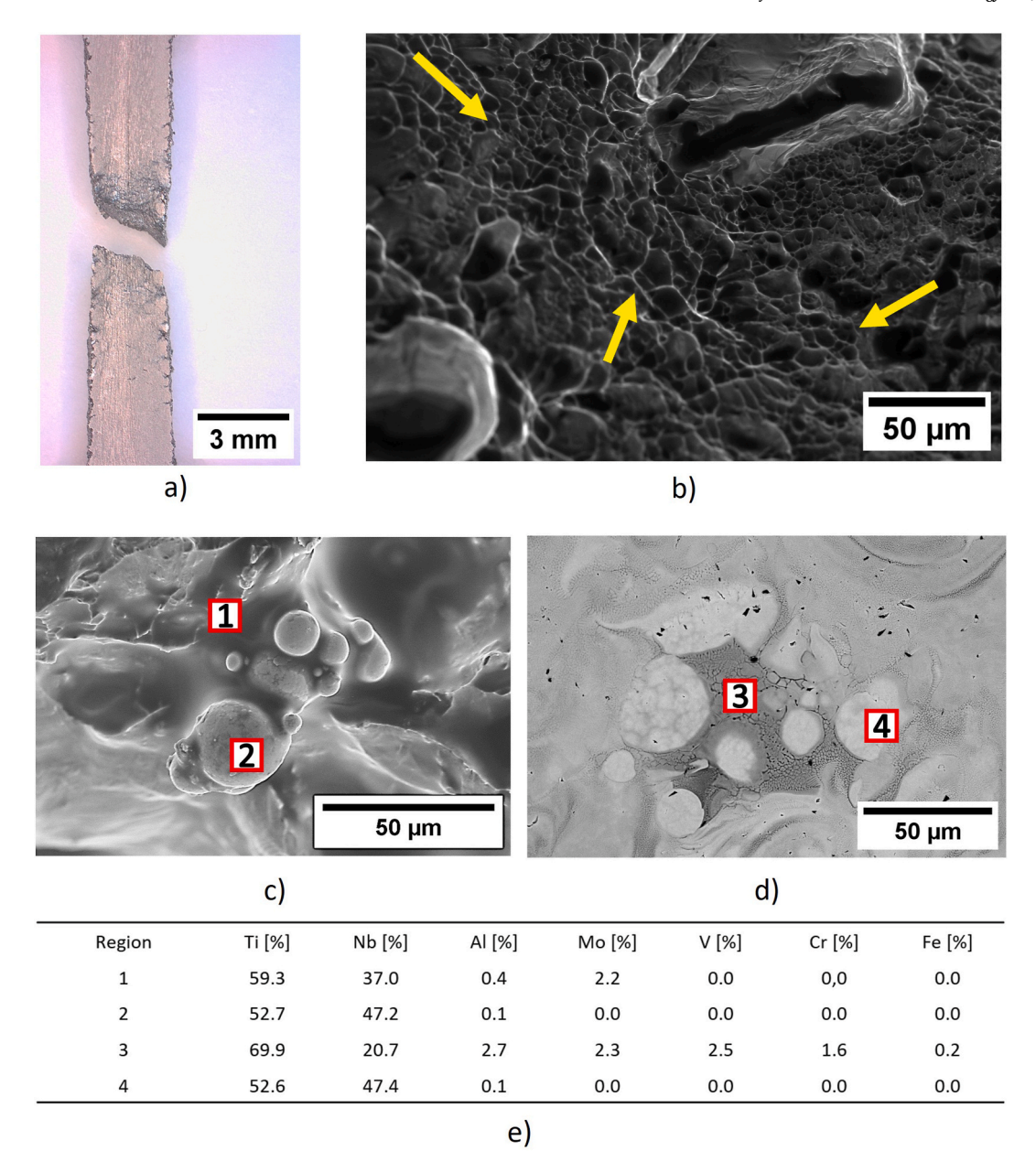


Fig. 12. In (a), stereoscope image of the fracture. In (b), the SEM-SE image displays dimples. In (c) and (d), SEM-SE and SEM-BSE micrographs of the unmelted Ti-42Nb particles. In (e), a compositional analysis using EDS is performed on the points presented in (c) and (d).

Table 3 A comparison of Ti–42Nb and Ti-5553 alloys produced by additive manufacturing with the Hybrid Titanium Alloy studied in this work.

Material	E (GPa)	σ _{0.2} (MPa)	UTS (MPa)	ε _f (%)
Ti-42Nb	70.9 ± 4.1^a	481 ± 9 [13]	615.7 ± 12.9	29.8 ± 1.8
Ti-5553	97.5 ± 4.9^{a}	613 ± 12	711.8 ± 19.1	26.2 ± 2.6
Mix Recycled Ti-42 Nb + Ti-5553 (Present Study)	79.9 ± 4.9^{a}	531 ± 5	725.1 ± 15.9	23.4 ± 2.4
Mix Virgin Ti-42 Nb + Ti-5553 (Present Study)	74.4 ± 4.3^{a}	503 ± 61	668.1 ± 18.5	27.0 ± 1.5

^a Pulse-echo ultrasound technique.

Declaration of competing interest

The authors declare that they have no known competing financial interests or personal relationships that could have appeared to influence the work reported in this paper.

Acknowledgments

The authors acknowledge the São Paulo State Research Foundation (FAPESP), grants # 2018/18293–8 and # 2022/10049–6, for its financial support and OmniTek Tecnologia for the technical assistance in additive manufacturing.

References

- Abdulhameed O, Al-Ahmari A, Ameen W, Mian SH. Additive manufacturing: challenges, trends, and applications. Adv Mech Eng 2019;11.
- [2] de Araujo APM, Kiminami CS, Uhlenwinkel V, Gargarella P. Processability of recycled quasicrystalline Al-Fe-Cr-Ti composites by selective laser melting - a statistical approach. Materialia (Oxf). 2022;22.
- [3] Gerday A-F. Mechanical behavior of Ti-5553 alloy modeling of representative cells, doctorate in science and engineering. Université de Liège; 2009.
- [4] Gibson I, Rosen D, Stucker B, Khorasani M. Additive manufacturing technologies. Cham: Springer International Publishing; 2021.
- [5] Gorji NE, O'Connor R, Brabazon D. XPS, SEM, AFM, and Nano-Indentation characterization for powder recycling within additive manufacturing process. IOP Conf Ser Mater Sci Eng 2021;1182:012025.
- [6] Moghimian P, Poirié T, Habibnejad-Korayem M, Zavala JA, Kroeger J, Marion F, Larouche F. Metal powders in additive manufacturing: a review on reusability and recyclability of common titanium, nickel and aluminum alloys. Addit Manuf 2021; 43:102017.
- [7] Moura LS, Vittoria GD, Gabriel AHG, Fonseca EB, Gabriel LP, Webster TJ, Lopes ÉSN. A highly accurate methodology for the prediction and correlation of mechanical properties based on the slimness ratio of additively manufactured tensile test specimens. J Mater Sci 2020;55:9578–96.
- [8] Pede D, Li M, Virovac L, Poleske T, Balle F, Müller C, Mozaffari-Jovein H. Microstructure and corrosion resistance of novel β-type titanium alloys manufactured by selective laser melting. J Mater Res Technol 2022;19:4598–612.
- [9] Pitassi D, Savoia E, Fontanari V, Molinari A, Luchin V, Zappini G, Benedetti M. Finite element thermal analysis of metal parts additively manufactured via selective laser melting. In: Finite element method - simulation, numerical analysis and solution techniques. InTech; 2018.
- [10] Ramachandiran N, Asgari H, Dibia F, Eybel R, Muhammad W, Gerlich A, Toyserkani E. Effects of post heat treatment on microstructure and mechanical properties of Ti5553 parts made by laser powder bed fusion. J Alloys Compd 2023; 938.
- [11] A.U. Rehman, K. Azher, A. Rehman, M. Shah, M.A. Mahmood, C.S. Tüfekci, M.U. Salamci, Additive manufacturing of Ti6Al4V using direct energy deposition: an elaborative approach of process modelling via computational fluid dynamics, n.d.
- [12] Sangali M, Cremasco A, Soyama J, Caram R, Contieri RJ. Selective laser melting of Ti-6Al-4V alloy: correlation between processing parameters, microstructure and corrosion properties. Mater Res 2023;26.

- [13] Schulze C, Weinmann M, Schweigel C, Keßler O, Bader R. Mechanical properties of a newly additive manufactured implant material based on Ti-42Nb. Materials 2018:11.
- [14] Sharma D, Kada SR, Fabijanic D, Parfitt D, Chen B, Roebuck B, Fitzpatrick ME, Barnett MR. The ageing response of direct laser deposited metastable β-Ti alloy, Ti–5Al–5Mo–5V–3Cr. Addit Manuf 2021;48:102384.
- [15] Sherov K, Ainabekova S, Kuanov I, Myrzakhmet B, Bekzhanov Y, Gabdyssalik R, Mazdubay A, Kamarov A, Sherov A. Research of temperature distribution in the process of thermo-frictional cutting of titanium alloy Ti-5553. Journal of Applied Engineering Science 2022;20:400–7.
- [16] Sri Maha Vishnu D, Sure J, Liu Y, Vasant Kumar R, Schwandt C. Electrochemical synthesis of porous Ti-Nb alloys for biomedical applications. Mater Sci Eng C 2019; 96:466–78.
- [17] Sun Y, Aindow M, Hebert RJ. The effect of recycling on the oxygen distribution in Ti-6Al-4V powder for additive manufacturing, Materials at High Temperatures 2018;35:217–24.
- [18] Wang YZ, Zhao YX, Gong FY, Dong JF, Maekawa K. Developing a threedimensional finite element analysis approach to simulate corrosion-induced concrete cracking in reinforced concrete beams. Eng Struct 2022;257.
- [19] Xiang Y, Zhang S, Wei Z, Li J, Wei P, Chen Z, Yang L, Jiang L. Forming and defect analysis for single track scanning in selective laser melting of Ti6Al4V. Appl Phys Mater Sci Process 2018;124.
- [20] Xin H, Sun WC, Fish J. Discrete element simulations of powder-bed sintering-based additive manufacturing. Int J Mech Sci 2018;149:373–92.
- [21] Yan W, Ma W, Shen Y. Powder sintering mechanisms during the pre-heating procedure of electron beam additive manufacturing. Mater Today Commun 2020; 25.
- [22] Yuan W, Chen H, Cheng T, Wei Q. Effects of laser scanning speeds on different states of the molten pool during selective laser melting: simulation and experiment. Mater Des 2020;189.
- [23] Zafari A, Chandran P, Xia K. Superior tensile properties in additively manufactured Ti alloys. Aust J Mech Eng 2021;19:602–8.
- [24] Zafari A, Lui EW, Jin S, Li M, Molla TT, Sha G, Xia K. Hybridisation of microstructures from three classes of titanium alloys. Mater Sci Eng 2020:788.
- [25] Zafari A, Xia K. Superior titanium from hybridised microstructures a new strategy for future alloys. Scripta Mater 2019;173:61–5.
- [26] Zhang F, Wang L, Yan S, Yu G, Chen J, He J, Yin F. Effect of Al content on microstructure and mechanical properties of atmosphere plasma sprayed AlxCoCrFeNi high-entropy alloy coatings under post-annealing. Surf Coat Technol 2022;446:128804.